Open Access

OBM Genetics

LIDSEN Publishing Inc.

Research Article

B_5N_{10} Nanocarrier Functionalized with Al, C, Si Atoms: A Drug Delivery Method for Infectious Disease Remedy

Fatemeh Mollaamin [1, *], Majid Monajjemi [2]

1. Department of Biomedical Engineering, Faculty of Engineering and Architecture, Kastamonu University, Kastamonu, Turkey; E-Mails: fmollaamin@kastamou.edu.tr; smollaamin@gmail.com
2. Department of Chemical Engineering, Central Tehran Branch, Islamic Azad University, Tehran, Iran; E-Mail: maj.monajjemi@iauctb.ac.ir

* **Correspondence:** Fatemeh Mollaamin; E-Mails: fmollaamin@kastamou.edu.tr; smollaamin@gmail.com

Academic Editor: Fabrizio Stasolla

Special Issue: New Advances in Neurodegenerative Diseases

OBM Genetics
2024, volume 8, issue 1
doi:10.21926/obm.genet.2401214

Received: November 27, 2023
Accepted: February 17, 2024
Published: February 21, 2024

Abstract

As proof has recommended a close connection between COVID-19 and neurodegenerative disorders, this article aims to investigate the chloroquine (CLQ) drug as the SARS-CoV-2's primary protease, which can prevent in vitro viral duplication of all diverse experiments to present. CLQ is an anti-viral drug enlarged by Pfizer, which can operate as an orally effective 3C-like protease inhibitor. In this study, CLQ has been assessed for its effectiveness against coronavirus by trapping it within a boron nitride nanocage (B_5N_{10}_NC) functionalized with specific atoms for drug delivery. This procedure relies on the principle of direct electron transfer and can be elucidated using density functional theory (DFT) in quantum mechanics methods. It was performed the theoretical method of the B3LYP/6-311+G(d,p) to account for the aptitude of B_5N_{10}_NC for grabbing CLQ drug via density of electronic states, nuclear quadrupole resonance, nuclear magnetic resonance, and thermodynamic specifications. Finally, the resulting amounts illustrated that using B_5N_{10}_NC functionalized with aluminum (Al), carbon (C), and silicon (Si) for adsorbing CLQ drug towards formation of CLQ@Al–

B_4N_{10}_NC, CLQ@C–B_4N_{10}_NC, CLQ@Si–B_4N_{10}_NC might provide the reasonable formula in drug delivery technique which can be fulfilled by quantum mechanics computations due to physicochemical properties of PDOS, NMR, NQR, and IR spectrum. An overview of recent developments in nanocage-based drug delivery systems will be provided, including the design of nanocages and atom-doped nanocages.

Keywords
Drug delivery; CLQ; COVID-19; Y–B_4N_{10} (Y = Al, C, Si)

1. Introduction

The intensity of the COVID-19 pandemic has waned since the beginning of 2022, in parallel with a significantly reduced risk for disease progression and death due to widespread vaccination, hybrid immunity, and the intrinsic low virulence of the Omicron subvariants [1-4]. Early therapies, including antiviral monoclonal antibodies and small molecules, have been approved to prevent disease progression and hospitalizations among high-risk outpatients with comorbidities [5]. Gottlieb et al. have investigated the early treatment of COVID-19 outpatients with oral antivirals or short daily infusions, which are considered a treatment strategy that assisted in turning the tides of the pandemic by reducing hospital admissions and mortality [6]. Furthermore, Kim et al. have indicated that while treatment options for patients with severe disease requiring hospitalization are now available, with corticosteroids emerging as the treatment of choice for critically ill patients, interventions administered early during infection to prevent disease progression and longer-term complications are urgently needed [7]. A particular therapy or vaccine is not available to battle SARS-CoV-2 [8]. Lately, antibodies have been almost all created in human cells and metamorphosed in animal cells, which are programs with many complicated tools [9, 10]. In addition, SARS-CoV-2 is a current major challenge for researchers, and they are still working on developing antiviral drugs against SARS-CoV-2 [11-13]. Currently, researchers and scientists are working on the development of a drug against COVID-19 in the following ways such as the prevention of self-assembly (structural proteins), viral replications (Nsps), viral entry, and the blocking of the signaling pathways required for viral infection [14-16].

Chloroquine with formula $C_{18}H_{26}ClN_3$ has antiviral and anti-inflammatory specifications and has been used in MERS-CoV, Zika virus, enterovirus EV-A71, OC43, influenza A H5N1, SARS-CoV, and SARS-CoV-2 infection treatment [17, 18].

Recently, several studies have explored the potential benefits of chloroquine or its derivative hydroxychloroquine, an affordable anti-malaria medication used for years in treating COVID-19 [19, 20].

Daolin et al. have exhibited that chloroquine, with a dual function in antiviral immunity, can be critical to note for introduction in the COVID-19 cure [21].

There is regard to augmenting the bioavailability and interval of operation for a medication to correct remedial outcomes. Drug delivery approach can alter a medication's pharmacokinetics and quality by providing it with diverse components, medication transfers, and medical tools [22-25].

Lee et al. indicated that protein-based nanocages are of specific interest because of their potential applicability as drug delivery carriers and their perfect and complex symmetry and ideal physical properties, which have stimulated researchers to engineer, modify, or mimic these qualities [26]. Amongst nanoparticles, boron nitride (BN) nanomaterials [27] have shown excellent physical and chemical properties [28] and a broad usage perspective in drug delivery systems [29].

In this work, it was concentrated on CLQ drug attached to functionalized B_4N_{10}_NC with Al, C, and Si atoms towards the formation of CLQ@Al–B_4N_{10}_NC, CLQ@C–B_4N_{10}_NC, CLQ@Si–B_4N_{10}_NC complexes for releasing the drug (Figure 1).

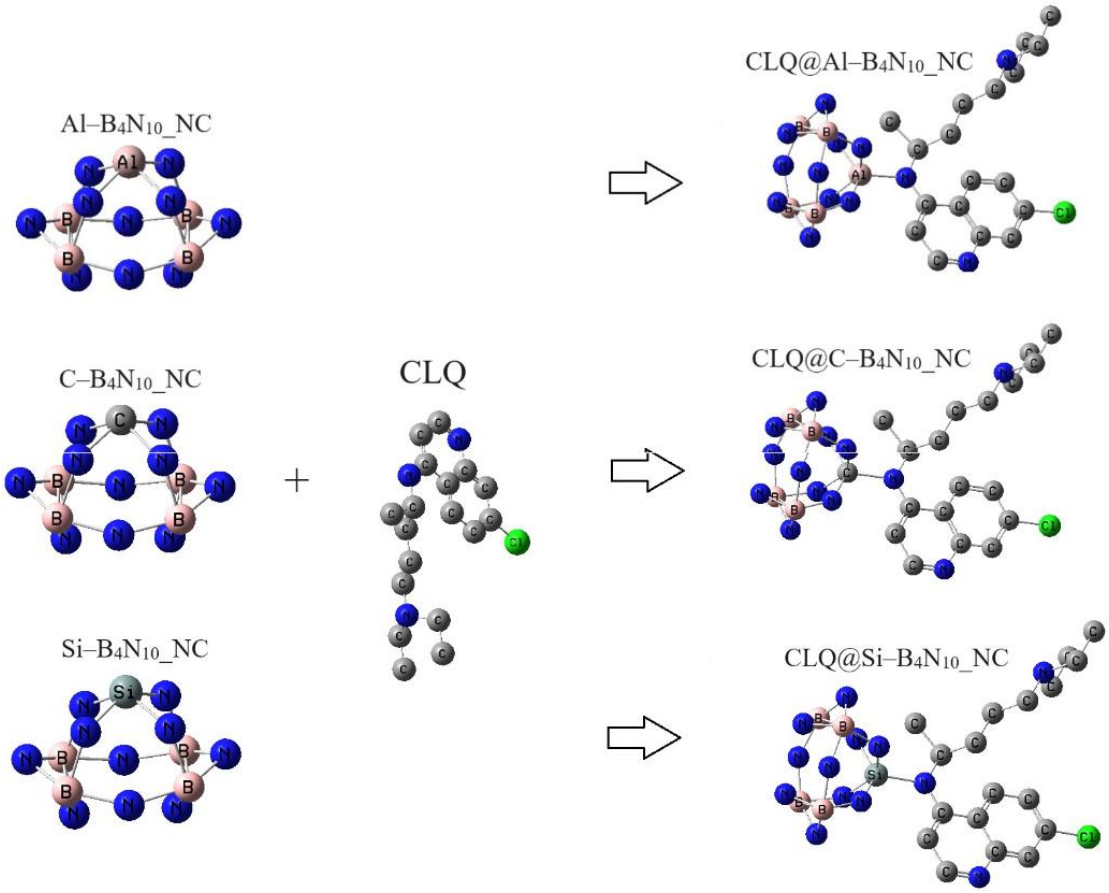

Figure 1 Carrying the CLQ by functionalized B_4N_{10}_NC with Al, C, and Si atoms towards the formation of CLQ@Al–B_4N_{10}_NC, CLQ@C–B_4N_{10}_NC, CLQ@Si–B_4N_{10}_NC complexes.

The propagation of medications into the cellular membrane is a significant phase in drug delivery methods. Exploring the COVID-19 drugs has recently drawn considerable regard to fighting its spread [30].

Research has shown that CLQ due to $B_{24}N_{24}$ nanocage can effectively help control COVID-19 disease. In addition, the nanocage decorated with silicon and aluminum has shown an appropriate drug delivery for CLQ owing to their larger energetic and electronic characteristics with CLQ [31].

2. Theoretical Background and Computational Methods

In this work, the structures of CLQ drug adsorbed on the Y–B_4N_{10} (Y = Al, C, Si) were minimized at the skeleton of density functional theory (DFT) [32, 33] accompanying the three-parameter

Becke's exchange [34] and Lee-Yang-Parr's correlation non-local functional [35], introduced as B3LYP level of theory and basis set of 6–311+G(d,p). Molecular modeling techniques are employed to elucidate the interaction process between the CLQ drug and Y–B_4N_{10} (Y = Al, C, Si), leading to the formation of CLQ@Al–B_4N_{10}_NC, CLQ@C–B_4N_{10}_NC, and CLQ@Si–B_4N_{10}_NC complexes, which serve as the drug delivery system for the treatment of COVID-19 disease (Figure 1).

In this research, the Onsager pattern was carried out, which Frisch, Wong, and Wiberg extended by applying spherical cavities [36]. This model conveys a less accurate explanation of the solute/solvent interface, but it can lighten the assessment of energy derivatives in optimizing geometries and analyzing the frequencies. Furthermore, Cramer and Truhlar developed this pattern at the dipole level [37]. A cavity should have a physical impression like an Onsager design and have a mathematical susceptibility, as frequently occurred in other definitions of solvent influences [36]. So, the cavity must maintain the solvent and its neighbors as the greatest possibility section of the solute charge diffusion [38].

The discussion on the application of CNT in drug delivery programs involving various biomaterials containing DNA, proteins, and antibodies provides clarity in targeting specific cells, tissues, and organs. These substances might lightly interpenetrate cells, releasing medications straightly to the nucleus or cytoplasm. Drug-releasing platforms ameliorate the pharmacological and therapeutic profile and influence of the medication and pull down off-targets' occurrence [39].

In addition, the level of gauge, including atomic orbitals (GIAO), has been dedicated to working out the gauge difficulty in the measurement of nuclear magnetic shielding for [CLQ@X–B_4N_{10} (Y = Al, C, Si)] complexes using the DFT approach. A mass of quantum mechanical technics can accomplish discovering certain properties aspect of physicochemical specifications extracted from the minimized frame of CLQ drug attached to Y–B_4N_{10} (Y = Al, C, Si) consisting of the density of electrical states, electric potential, Bader charge distribution, vibrational computations, and nuclear magnetic resonance analysis owing to running a drug delivery model using Gaussian 16 revision C.01 program (Figure S1) [40].

3. Results and Discussion

In this work, the effect of CLQ drugs on COVID-19 treatment has been studied owing to attaching to the Y–B_4N_{10} (Y = Al, C, Si) complexes as the drug delivery techniques.

3.1 Projected Density of State (PDOS)

Figure 2(a-d) introduces the PDOS of CLQ drug, Al–B_4N_{10}, C–B_4N_{10}, and Si–B_4N_{10}, respectively. It is evident from the figure that after the adsorption of CLQ drug on the Y–B_4N_{10} (Y = Al, C, Si), there is a significant contribution of *p*-orbitals of Al, C, Si, N, and Cl atoms in the unoccupied stage. The electronic structure of the CLQ drug attached to the Y–B_4N_{10} (Y = Al, C, Si) nanocage was evaluated to explain the interfacial electronic parameters using quantum methods.

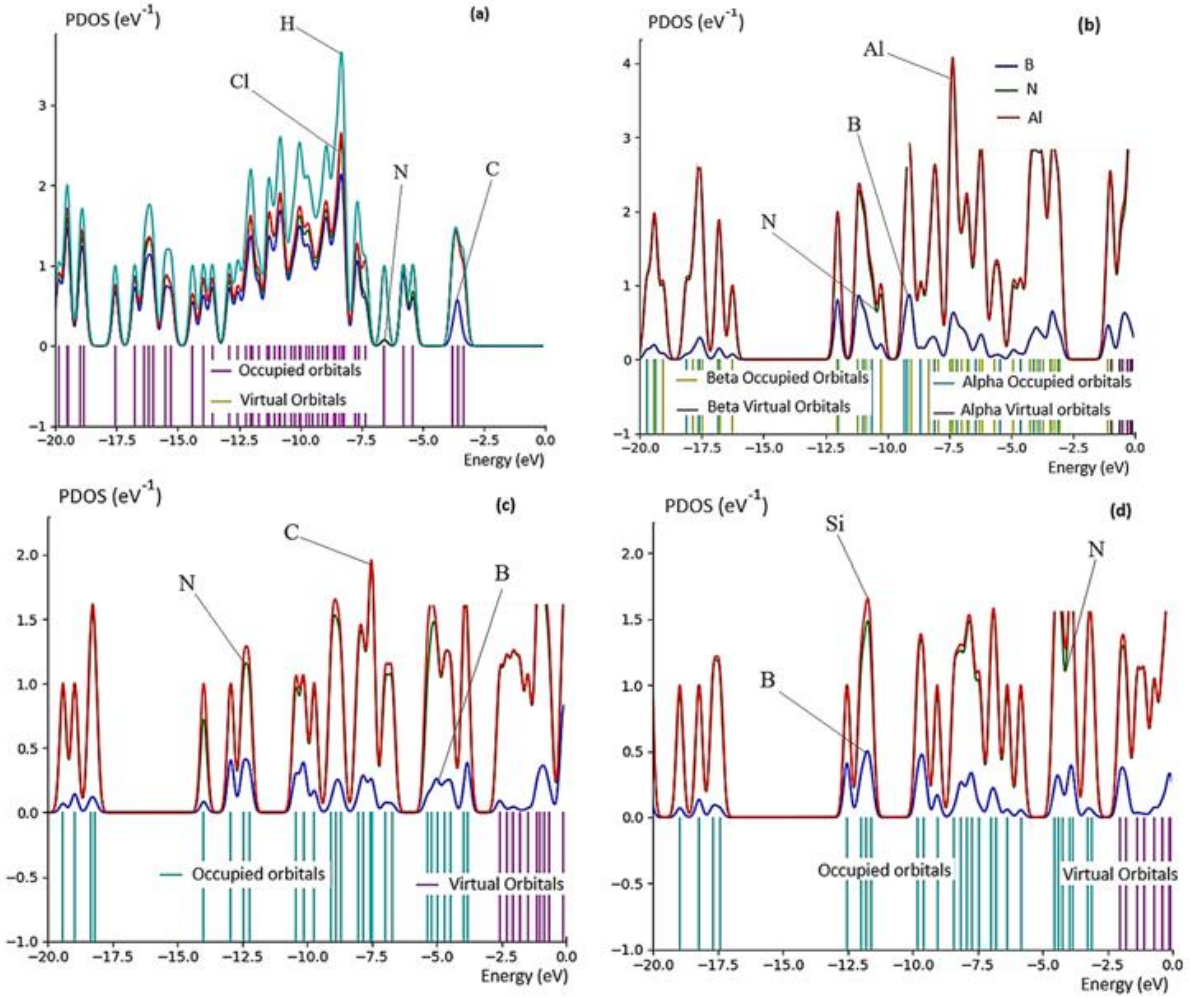

Figure 2 Electronic properties of PDOS for a) CLQ drug absorbed on b) Al–B_4N_{10}, c) C–B_4N_{10}, and d) Si–B_4N_{10}.

Population analysis and PDOS reveal that the C, N, and Cl atoms of CLQ form bonds with Y–B_4N_{10} (Y = Al, C, Si), suggesting their capability to attract additional electrons from neighboring elements. Furthermore, the existence of covalent features for [CLQ@Y–B_4N_{10} (Y = Al, C, Si)] complex has shown the equal energy content and configuration of the PDOS for the *p* orbitals of Al, C, Si, N, and Cl atoms (Figure 2a-b). There, the graph of PDOS has discovered that the *p* states of the adsorption of C, N, and Cl atoms on the Y–B_4N_{10} (Y = Al, C, Si) are significant through the conduction band.

The CLQ drug states adsorbed onto Y–B_4N_{10} (Y = Al, C, Si) complexes have more contribution at the middle of the conduction band between -5eV to -15eV, while contribution of C, N, Cl states in CLQ drug are expanded and close together (Figure 2a), and Al states in Al–B_4N_{10}_NC (Figure 2b), C in C–B_4N_{10}_NC (Figure 2c) and Si in Si–B_4N_{10}_NC (Figure 2d) approximately have the most contributions. The mentioned consequences display that the principal complex and a certain degree of covalent traits can ameliorate the straight conducting band gap of CLQ drug absorbing on the Y–B_4N_{10} (Y = Al, C, Si) complexes.

The nanocarrier would not substantially alter the properties of the drug. Previous studies [41, 42] also evaluated electrical conductivity and electronic sensitivity.

3.2 Nuclear Magnetic Resonance (NMR)

The NMR data of shielding tensors (ppm) consisting of isotropic (σ_{iso}) and anisotropic (σ_{aniso}) for CLQ drug linked to X–B_4N_{10} (X = Al, C, Si) complexes were computed (Table 1). The accomplished consequences have demonstrated the "SCF/GIAO" magnetic shielding tensor for Al, C, Si, N, and Cl atoms, discovering the active zone of CLQ material as the medication for viral disease therapy. The estimations have been run on the "B3LYP/6–311+G(d,p)" level of theory using the Gaussian 16 revision C.01 program [40] and have been reported (Table 1).

Table 1 Nuclear magnetic resonance (NMR) tensors (ppm) for CLQ drug attached to Al–B_4N_{10}_NC, C–B_4N_{10}_NC, and Si–B_4N_{10}_NC by quantum methods. SCF GIAO Magnetic shielding tensors (ppm) [43].

CLQ			Al-B_4N_{10}_NC			C-B_4N_{10}_NC			Si-B_4N_{10}_NC		
Atom	σ_{iso}	σ_{aniso}	Atom	σ_{iso}	σ_{aniso}	Atom	σ_{iso}	σ_{aniso}	Atom	σ_{iso}	σ_{aniso}
C1	132.52	130.65	B1	96.71	82.91	B1	103.95	91.64	B1	69.65	66.87
C2	134.71	115.73	N2	259.30	626.11	N2	111.66	621.75	N2	211.97	928.02
C3	154.14	132.97	N3	58.49	79.64	N3	1655.31	2921.16	N3	890.97	2652.00
C4	133.90	120.89	B4	105.97	72.42	B4	99.38	130.29	B4	93.00	40.07
C5	129.01	112.43	B5	94.94	58.17	B5	111.94	44.71	B5	56.79	52.74
C6	121.43	90.28	B6	78.48	78.26	B6	111.96	63.24	B6	55.44	76.88
C7	135.35	119.43	N7	180.32	573.04	N7	268.02	362.56	N7	147.71	1114.40
C8	145.64	85.83	N8	79.95	253.36	N8	557.61	1335.78	N8	1417.29	2153.41
C9	124.85	112.78	N9	460.09	832.80	N9	601.87	1305.01	N9	588.36	4046.60
N10	76.90	440.22	N10	558.79	717.03	N10	877.08	1752.31	N10	575.52	2937.29
N11	236.30	37.80	N11	512.23	941.85	N11	1094.84	1854.46	N11	88.60	3677.85
C12	179.56	34.90	N12	283.32	712.10	N12	637.42	1166.30	N12	300.50	2936.03
C13	204.91	29.29	Al13	488.58	206.97	C13	99.65	87.81	Si13	670.58	157.49
C14	198.50	27.14	N14	28.48	599.67	N14	35.63	1510.04	N14	123.22	1007.9
C15	200.92	22.42	N15	21.33	591.87	N15	262.85	1199.51	N15	40.17	1170.06
C16	179.88	55.74									
N17	274.67	37.68									
C18	184.27	51.36									
C19	208.57	23.61									
C20	186.65	40.51									
C21	208.71	17.64									
Cl22	920.80	169.33									

The [CLQ@Y–B_4N_{10} (Y = Al, C, Si)] complexes have reflected the significance of chemical shielding consisting of σ_{iso} and σ_{aniso} (ppm) for diverse elements of B, Al, C, Si, N, and Cl atoms in the active zones of the system owing to the NMR curve (Table 1). Furthermore, the ^{13}C–NMR considerations on CLQ drug have approved the active zones of this compound owing to unraveling the most electron donor elements during CLQ drug adsorption onto X–B_4N_{10} (X = Al, C, Si) complexes, which expose the major shift in tetramethylsilane (TMS) using quantum methods (Figure 3a-d).

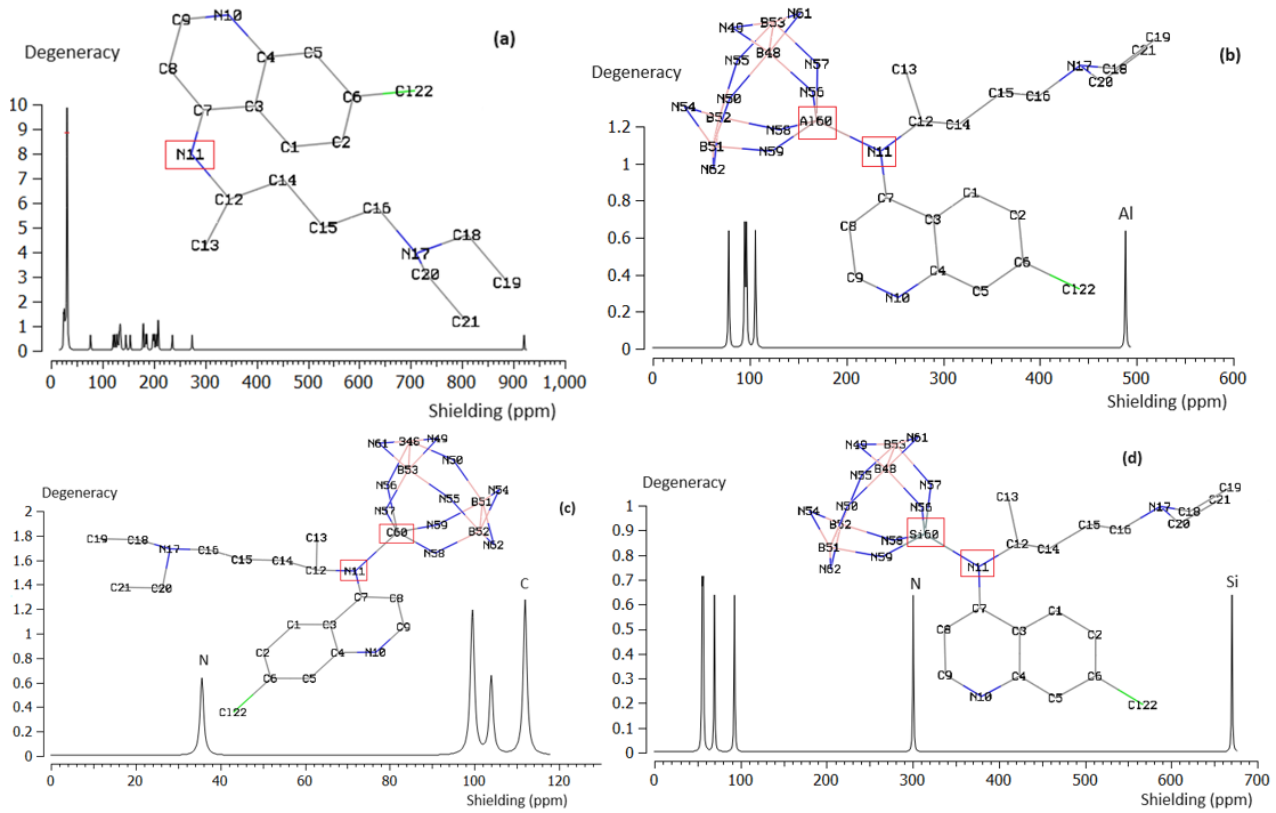

Figure 3 NMR spectra for a) CLQ drug, b) CLQ@Al–B_4N_{10}_NC, c) CLQ@C–B_4N_{10}_NC, d) CLQ@Si–B_4N_{10}_NC.

The progress of impressive DFT methods, including electronic correlation effects, has been illustrated as a significant key in shielding computations. By DFT theory, which measures N^2 (N = number of electrons), it is feasible to compute shielding in molecular systems of practical interest consisting of electronic correlation impacts. Furthermore, new DFT approaches with linear scaling are accessible, and these will supply further developments in implementing these techniques to compute magnetic shielding in large groups [43].

The actual computation of these impacts is quite puzzling because any model that seeks to indicate these interactions must estimate both the electromagnetic iterations produced by the solvent molecules and their dynamic parameters. Based on the theory, this skeleton analyses the solvent effects on magnetic shielding. Recently, Emwas et al. have investigated NMR spectroscopy, which can be a significant method in drug design because of its characterizations [44].

The most alterations were declared for atoms of N11 in CLQ drug (Figure 3a), N11, Al60 in CLQ@Al–B_4N_{10} (Figure 3b), N11, C60 in CLQ@C–B_4N_{10} (Figure 3c), N11, Si60 in CLQ@Si–B_4N_{10} (Figure 3d).

3.3 Nuclear Quadrupole Resonance (NQR)

The NQR spectra can prepare exact data on active groups' structural and composition properties in biological reactions [45]. It presents a special probability of identifying the quadrupole coupling constants and impressive charges, which gives us knowledge of the electronic structure of the system. NQR spectrums become visible to propose an intense approach for inquiring about diverse

chemical influences in the solid phase of many nitrogen-possessing substances. Analyzing the quadrupole coupling constants of nitrogen atoms permits an assessment of the electron density distribution on the nitrogen nuclei. It authorizes the analysis of charge distribution in chemical bonding dealing with nitrogen atoms.

So, "nuclear quadrupole resonance" or "NQR" was evaluated for CLQ drug trapped by the surface of Y–B_4N_{10} (Y = Al, C, Si) nanocages towards the formation of [CLQ@Y–B_4N_{10} (Y = Al, C, Si)] complexes based on the "nuclear quadrupole moment", and the "electric field gradient" or "EFG" (Table 2) [45].

Table 2 Electric potential (E_p/a.u.) and Bader charge (Q/coulomb) through NQR calculation for functionalized elements of CLQ drug attached to Al–B_4N_{10}, C–B_4N_{10}, and Si–B_4N_{10} nanocages.

CLQ			Al-B_4N_{10}_NC			C-B_4N_{10}_NC			Si-B_4N_{10}_NC		
Atom	Q	E_p	Atom	Q	E_p	Atom	Q	E_p	Atom	Q	E_p
C1	0.01	-14.54	B1	-0.42	-11.30	B1	0.29	-11.27	B1	0.33	-11.26
C2	0.00	-14.54	N2	0.32	-18.14	N2	-0.15	-18.09	N2	-0.16	-18.11
C3	-0.04	-14.53	N3	-1.49	-18.12	N3	-0.13	-18.07	N3	-0.16	-18.10
C4	0.09	-14.51	B4	-0.37	-11.30	B4	0.29	-11.26	B4	0.33	-11.27
C5	0.04	-14.55	B5	-0.54	-11.30	B5	0.30	-11.28	B5	0.33	-11.26
C6	0.00	-14.50	B6	-0.26	-11.28	B6	0.29	-11.27	B6	0.33	-11.26
C7	0.10	-14.47	N7	0.58	-18.14	N7	-0.15	-18.09	N7	-0.16	-18.12
C8	0.04	-14.57	N8	1.57	-18.13	N8	-0.13	-18.08	N8	-0.15	-18.09
C9	0.10	-14.53	N9	0.47	-18.20	N9	-0.10	-18.08	N9	-0.33	-18.18
N10	-0.28	-18.14	N10	-0.24	-18.20	N10	-0.10	-18.09	N10	-0.33	-18.17
N11	-0.07	-18.01	N11	-0.02	-18.18	N11	-0.09	-18.08	N11	-0.31	-18.16
C12	0.12	-14.46	N12	0.20	-18.18	N12	-0.10	-18.07	N12	-0.32	-18.15
C13	0.02	-14.52	Al13	-0.00	-43.70	C13	0.11	-14.53	Si13	0.96	-48.39
C14	0.02	-14.52	N14	0.73	-18.12	N14	-0.14	-18.08	N14	-0.18	-18.12
C15	0.01	-14.52	N15	0.46	-18.13	N15	-0.14	-18.08	N15	-0.18	-18.12
C16	0.08	-14.51									
N17	-0.25	-18.10									
C18	0.08	-14.51									
C19	0.00	-14.55									
C20	0.08	-14.51									
C21	0.01	-14.54									
Cl22	-0.10	-63.31									

Furthermore, in Figure 4(a-d), the electric potential versus Bader charge was plotted to depict the attachment of the CLQ drug onto Y–B_4N_{10} (Y = Al, C, Si) nanocages, employing theoretical methods for measurement.

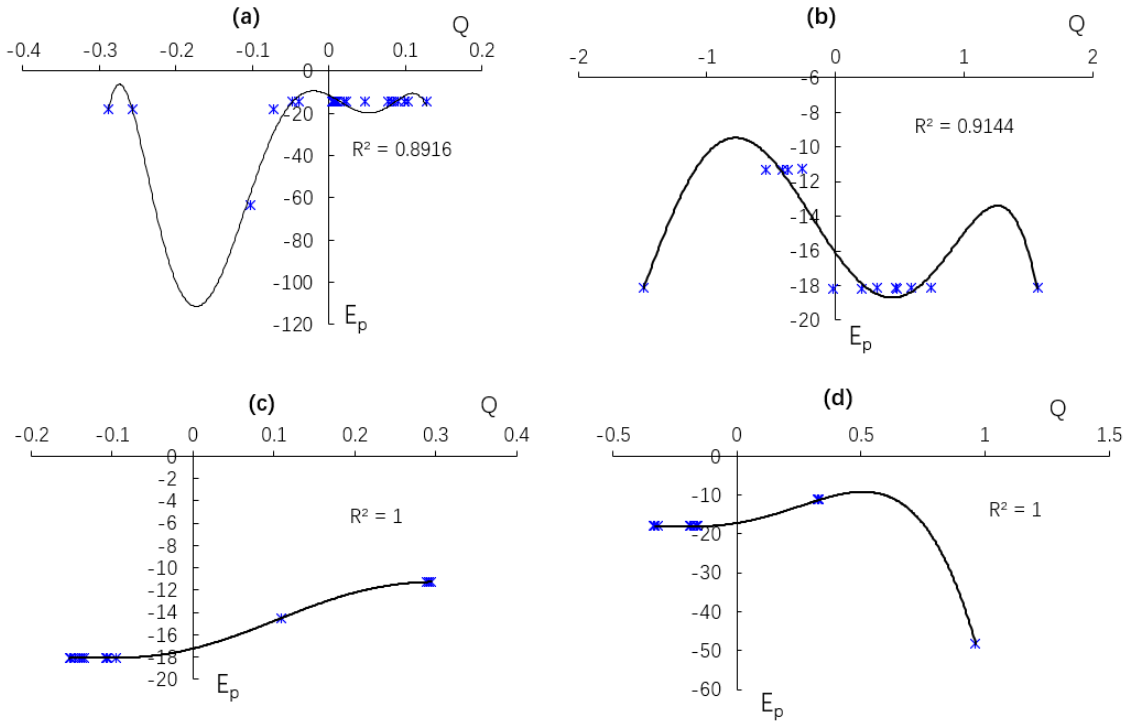

Figure 4 Electric potential (E_p/a.u.) versus Bader charge (Q/coulomb) through NQR calculation for **a)** CLQ drug, **b)** CLQ@Al–B_4N_{10}_NC, **c)** CLQ@C–B_4N_{10}_NC, **d)** CLQ@Si–B_4N_{10}_NC.

Figure 4(a) exhibited the fluctuation of the charge distribution for all atoms in the CLQ drug towards understanding which atoms have more electron donating tendency in the attachment to the Y–B_4N_{10} (Y = Al, C, Si) complexes. On the other hand, element N in the CLQ drug acts like an electron donor, which has a high energy orbital with one or more electrons. So, in Y–B_4N_{10} (Y = Al, C, Si) complexes, the elements of Al, C, and Si can be considered electron acceptors with a low energy orbital with one or more vacancies (Figure 4b, c, d).

The influence of the linkage between N11 in the CLQ drug (Figure 4a) with a relation coefficient (R^2 = 0.8916) and Al13, C13, and Si13 in Al–B_4N_{10}_NC (Figure 4b) with R^2 = 0.9144, C–B_4N_{10}_NC (Figure 4c), and Si–B_4N_{10}_NC (Figure 4d) complexes with R^2 = 1, respectively, during the adsorption of CLQ was presented. These relationships were determined based on the data on E_p obtained from NQR spectroscopy. The competence of Y–B_4N_{10} (Y = Al, C, Si) complexes for sensing CLQ is oscillated by their selectivity and sensitivity, which can indicate the yield of these materials as the engaged detectors.

3.4 Spectroscopy of Infrared (IR)

The IR spectra through some computations were completed for CLQ drug (Figure 5a) attached to Y–B_4N_{10} (Y = Al, C, Si) complexes by DFT approach to catch a more stable system accompanying thermodynamic attributes. Therefore, it has been simulated the several complexes containing CLQ@Al–B_4N_{10}_NC (Figure 5b), CLQ@C–B_4N_{10}_NC (Figure 5c), CLQ@Si–B_4N_{10}_NC (Figure 5d), respectively.

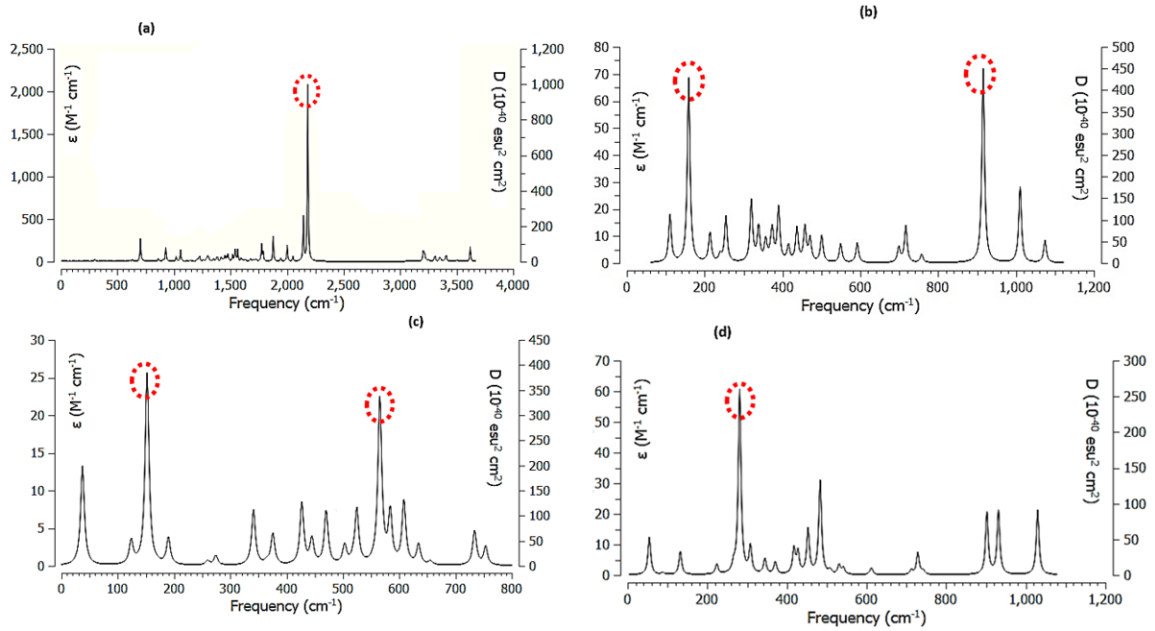

Figure 5 Frequency (cm^{-1}) amounts of IR spectrums for **a)** CLQ drug, **b)** CLQ@Al–B_4N_{10}_NC, **c)** CLQ@C–B_4N_{10}_NC, **d)** CLQ@Si–B_4N_{10}_NC (Note: Some sharpest peak in the IR spectra have been drawn dotted circles).

The graph of Figure 5(a) was shown in the frequency limitation across 500-3500 cm^{-1} for CLQ drug with a sharp peak around 2183.43 cm^{-1}. Figure 5(b) shows the frequency range between 100-1500 cm^{-1} for CLQ@Al–B_4N_{10}_NC with two sharp peaks around 158.81 and 915.64 cm^{-1}. Figure 5(c) indicates the fluctuation of frequency between 50-750 cm^{-1} for CLQ@C–B_4N_{10}_NC with sharp peaks around 37.34, 152.01, and 565.57 cm^{-1}. Figure 5(d) has shown the fluctuation of frequency between 100-1100 cm^{-1} for CLQ@Si–B_4N_{10}_NC with sharp peaks around 281.19, 483.33, 902.26, 931.18 and 1029.57 cm^{-1}.

The perspective of Figure 5(a-d) introduces the proof for different frequencies of [CLQ@Y–B_4N_{10} (Y = Al, C, Si)] complexes, which indicate the active sites in the CLQ drug and functionalized atoms in Y–B_4N_{10} (Y = Al, C, Si) that can transfer the charge of electrons in polar CLQ into the Y–B_4N_{10} (Y = Al, C, Si) complexes.

In addition, Table 3, through the thermodynamic specifications, concluded that Y–B_4N_{10} (Y = Al, C, Si), due to the adsorption of CLQ drug, might be a more efficient sensor for a drug delivery system.

Table 3 Thermodynamic characters thermal energy(ΔE°), thermal enthalpy (ΔH°), Gibbs free energy (ΔG°), entropy (S°) and dipole moment of CLQ drug, CLQ@Al–B_4N_{10}_NC, c) CLQ@C–B_4N_{10}_NC, CLQ@Si–B_4N_{10}_NC using CAM-B3LYP/6-311+G(d,p), LANL2DZ calculation.

Compound	ΔE° × 10^{-4} (kcal/mol)	ΔH° × 10^{-4} (kcal/mol)	ΔG° × 10^{-4} (kcal/mol)	S° (cal/K.mol)	Dipole moment (Debye)
CLQ drug	-821.875	-821.875	-821.913	129.091	5.8364
CLQ@Al–B_4N_{10}	-55.0351	-55.0350	-55.0379	98.176	3.4260
CLQ@C–B_4N_{10}	-42.3537	-42.3536	-42.3566	99.093	1.4160
CLQ@Si–B_4N_{10}	-57.9539	-57.9538	-57.9568	99.252	1.2968

Polarization is a practical basis in the enumerations, indicating notable prosperity in quantum-theoretical techniques. The outcomes of the mentioned perceptions indicate that CLQ is attached to the Y–B_4N_{10} (Y = Al, C, Si) complex, which is persuaded by a mutation in the polarization of the ambiance. It can be found that growth in the dielectric constant augments the endurance and turnover of this medication for curing the COVID-19 viral malady.

The adsorption process of CLQ drug on the surface of functionalized B_4N_{10}_NC by Al, C, and Si elements is affirmed by the quantity:

$$\Delta G_{\mathrm{R}}^{o} = \Delta G_{\mathrm{CLQ@Y\text{–}B4N10\_NC}}^{o} - \left(\Delta G_{\mathrm{CLQ-adsorbed}}^{o} + \Delta G_{\mathrm{Y\text{–}B4N10\_NC}}^{o}\right); \mathrm{Y} = \mathrm{Al, C, Si}$$

Figure 6 has shown the fluctuation of ΔG^{o} versus dipole moment for different functionalized nanocages of Al–B_4N_{10}_NC, C–B_4N_{10}_NC, and Si–B_4N_{10}_NC as electron acceptors (adsorbents) for trapping CLQ drug as an electron donor (adsorbate) during interaction process as a promising drug delivery system (Figure 6).

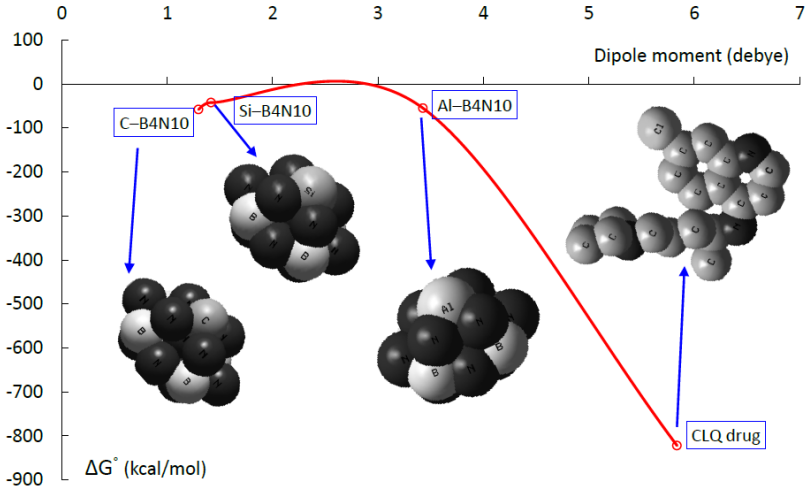

Figure 6 The Gibbs free energy ($\Delta G_{\mathrm{R}}^{o}$) versus dipole moment (Debye) for CLQ drug, Al–B_4N_{10}_NC, C–B_4N_{10}_NC, Si–B_4N_{10}_NC complexes.

As seen in Table 3, all accounted ΔG^{o} amounts of Al–B_4N_{10}_NC, C–B_4N_{10}_NC, and Si–B_4N_{10}_NC are close, which can demonstrate an appropriate potential of these functionalized nanocages for CLQ drug adsorption as a drug delivery technique.

4. Conclusions

CLQ drug has motivated scientists to investigate the clinical therapy of viral coronavirus malady (COVID-19) using linkage to the B_5N_{10}_NC, which can engage an impressive drug delivery approach due to PDOS, NMR, IR, NQR data analysis on the optimized structure extracted from DFT measurements. The complexes of Si–B_4N_{10}_NC > Al–B_4N_{10}_NC > and C–B_4N_{10}_NC are more electrophilic compared to both the pristine B_5N_{10}_NC nanocage and single CLQ. This proves that the nanocage-CLQ interaction enhanced electrophilicity. The adsorption of the drug onto the nanocage increased in the dipole moment of the complex. This is a privilege in drug delivery in a biological system. The structures had negative electrophilicity-based charge transfers. Therefore, the drug can result in an electron donor, while the doped nanocage is an electron acceptor. Doped nanocages of

boron nitride can demonstrate higher chloroquine delivery efficiency than the pristine nanocage, considering higher thermochemical properties and greater electromagnetic specifications.

Acknowledgments

In successfully completing this paper and its research, the authors are grateful to Kastamonu University.

Author Contributions

Fatemeh Mollaamin: Conceptualization and idea, Methodology, Software, Validation, Formal analysis, Investigation, Data Curation, Writing-original draft preparation, Visualization, Supervision, Project administration. Majid Monajjemi: Methodology, Software, Formal analysis, Investigation, Data Curation, Writing-review and editing, Visualization, Resources.

Funding

This research received no external funding.

Competing Interests

The authors declare that no competing interests exist.

Additional Materials

The following additional materials are uploaded at the page of this paper.

1. Figure S1: The scheme of drug delivery status by doped boron nitride nanocages of Al, C, Si towards releasing CLQ on the body cells for promising the COVID-19 treatment.

References

1. Sharma A, Tiwari S, Deb MK, Marty JL. Severe acute respiratory syndrome coronavirus-2 (SARS-CoV-2): A global pandemic and treatment strategies. Int J Antimicrob Agents. 2020; 56: 106054.
2. Hu B, Guo H, Zhou P, Shi ZL. Characteristics of SARS-CoV-2 and COVID-19. Nat Rev Microbiol. 2021; 19: 141-154.
3. Anand U, Cabreros C, Mal J, Ballesteros F, Sillanpää JM, Tripathi V, et al. Novel coronavirus disease 2019 (COVID-19) pandemic: From transmission to control with an interdisciplinary vision. Environ Res. 2021; 197: 111126.
4. Rana R, Kant R, Huirem RS, Bohra D, Ganguly NK. Omicron variant: Current insights and future directions. Microbiol Res. 2022; 265: 127204.
5. Taylor PC, Adams AC, Hufford MM, De La Torre I, Winthrop K, Gottlieb RL. Neutralizing monoclonal antibodies for treatment of COVID-19. Nat Rev Immunol. 2021; 21: 382-393.
6. Rottlieb RL, Vaca CE, Paredes R, Mera J, Webb BJ, Perez G, et al. Early remdesivir to prevent progression to severe COVID-19 in outpatients. N Engl J Med. 2022; 386: 305-315.
7. Kim PS, Read SW, Fauci AS. Therapy for early COVID-19: A critical need. JAMA. 2020; 324: 2149-2150.

8. Plavec Z, Domanska A, Liu X, Laine P, Paulin L, Varjosalo M, et al. SARS-CoV-2 production, purification methods and UV inactivation for proteomics and structural studies. Viruses. 2022; 14: 1989.
9. Zabidi NZ, Liew HL, Farouk IA, Puniyamurti A, Yip AJ, Wijesinghe VN, et al. Evolution of SARS-CoV-2 variants: Implications on immune escape, vaccination, therapeutic and diagnostic strategies. Viruses. 2023; 15: 944.
10. Yarovaya OI, Shcherbakov DN, Borisevich SS, Sokolova AS, Gureev MA, Khamitov EM, et al. Borneol ester derivatives as entry inhibitors of a wide spectrum of SARS-CoV-2 viruses. Viruses. 2022; 14: 1295.
11. Majeed A, Zhang X. On the adoption of modern technologies to fight the COVID-19 pandemic: A technical synthesis of latest developments. COVID. 2023; 3: 90-123.
12. Bonaccorsi G, Pierri F, Cinelli M, Flori A, Galeazzi A, Porcelli F, et al. Economic and social consequences of human mobility restrictions under COVID-19. Proc Natl Acad Sci USA. 2020; 117: 15530-15535.
13. Barakat A, Mostafa A, Ali M, Al-Majid AM, Domingo LR, Kutkat O, et al. Synthesis and in vitro evaluation of spirooxindole-based phenylsulfonyl moiety as a candidate anti-SAR-CoV-2 and MERS-CoV-2 with the implementation of combination studies. Int J Mol Sci. 2022; 23: 11861.
14. Zeng F, Huang Y, Guo Y, Yin M, Chen X, Xiao L, et al. Association of inflammatory markers with the severity of COVID-19: A meta-analysis. Int J Infect Dis. 2020; 96: 467-474.
15. Monajjemi M, Mollaamin F, Shojaei S. An overview on coronaviruses family from past to COVID-19: Introduce some inhibitors as antiviruses from Gillan's plants. Biointerface Res Appl Chem. 2020; 10: 5575-5585.
16. Bibi S, Khan MS, El-Kafrawy SA, Alandijany TA, El-Daly MM, Yousafi Q, et al. Virtual screening and molecular dynamics simulation analysis of Forsythoside A as a plant-derived inhibitor of SARS-CoV-2 3CLpro. Saudi Pharm J. 2022; 30: 979-1002.
17. Wang M, Cao R, Zhang L, Yang X, Liu J, Xu M, et al. Remdesivir and chloroquine effectively inhibit the recently emerged novel coronavirus (2019-nCoV) in vitro. Cell Res. 2020; 30: 269-271.
18. Touret F, de Lamballerie X. Of chloroquine and COVID-19. Antiviral Res. 2020; 177: 104762.
19. Colson P, Rolain JM, Lagier JC, Brouqui P, Raoult D. Chloroquine and hydroxychloroquine as available weapons to fight COVID-19. Int J Antimicrob Agents. 2020; 55: 105932.
20. Shahriari S, Monajjemi M, Mollaamin F. Determination of proteins specification with SARS-COVID-19 based ligand designing, J. Chil. Chem. Soc. 2022; 67: 5468-5476.
21. Tang D, Li J, Zhang R, Kang R, Klionsky DJ. Chloroquine in fighting COVID-19: Good, bad, or both? Autophagy. 2020; 16: 2273-2275.
22. Shahriari S, Monajjemi M, Zare K. Penetrating to cell membrane bacteria by the efficiency of various antibiotics (clindamycin, metronidazole, azithromycin, sulfamethoxazole, baxdela, ticarcillin, and clavulanic acid) using S-NICS theory. Biointerface Res. Appl. Chem. 2018; 8: 3219 -3223.
23. Singh AP, Biswas A, Shukla A, Maiti P. Targeted therapy in chronic diseases using nanomaterial-based drug delivery vehicles. Signal Transduct Target Ther. 2019; 4: 33.
24. Khalili Hadad B, Mollaamin F, Monajjemi M. Biophysical chemistry of macrocycles for drug delivery: A theoretical study. Russ Chem Bull. 2011; 60: 238-241.
25. Mollaamin F. Physicochemical investigation of anti-COVID19 drugs using several medicinal plants. J Chil Chem Soc. 2022; 67: 5537-5546.

26. Lee EJ, Lee NK, Kim IS. Bioengineered protein-based nanocage for drug delivery. Adv Drug Deliv Rev. 2016; 106: 157-171.
27. Mollaamin F. Computational Methods in the Drug Delivery of Carbon Nanocarriers onto Several Compounds in Sarraceniaceae Medicinal Plant as Monkeypox Therapy. Computation. 2023; 11: 84.
28. Pan D, Su F, Liu H, Ma Y, Das R, Hu Q, et al. The properties and preparation methods of different boron nitride nanostructures and applications of related nanocomposites. Chem Rec. 2020; 20: 1314-1337.
29. Mollaamin F, Shahriari S, Monajjemi M. Monkeypox disease treatment by tecovirimat adsorbed onto single-walled carbon nanotube through drug delivery method, J. Chil. Chem. Soc. 2023; 68: 5796-5801.
30. Ghaed-Sharaf T, Omidvar A. Exploring the permeability of COVID-19 drugs within the cellular membrane: A molecular dynamics simulation study. Phys Chem Chem Phys. 2022; 24: 6215-6224.
31. Alharthy KM, Alsaffar MF, Althurwi HN, Albaqami FF, Abass RR, Alawi AM, et al. Boron nitride nanocage as drug delivery systems for chloroquine, as an effective drug for treatment of coronavirus disease: A DFT study. Inorg Chem Commun. 2023; 150: 110482.
32. Penz M, Tellgren EI, Csirik MA, Ruggenthaler M, Laestadius A. The structure of density-potential mapping. Part I: Standard density-functional theory. ACS Phys Chem Au. 2023; 3: 334-347.
33. Mourik TV, Bühl M, Gaigeot MP. Density functional theory across chemistry, physics and biology. Philos Trans Royal Soc A. 2014; 372: 20120488.
34. Becke AD. Density-functional exchange-energy approximation with correct asymptotic behavior. Phys Rev A. 1988; 38: 3098-3100.
35. Lee C, Yang W, Parr RG. Development of the Colle-Salvetti correlation-energy formula into a functional of the electron density. Phys Rev B. 1988; 37: 785-789.
36. Onsager LJ. Electric moments of molecules in liquids. J Am Chem Soc. 1936; 58: 1486-1493.
37. Cramer CJ, Truhlar DG. PM3-SM3: A general parameterization for including aqueous solvation effects in the PM3 molecular orbital model. J Comput Chem. 1992; 13: 1089-1097.
38. Chambers CC, Hawkins GD, Cramer CJ, Truhlar DG. Model for aqueous solvation based on class IV atomic charges and first solvation shell effects. J Phys Chem. 1996; 100: 16385-16398.
39. Mollaamin F, Shahriari S, Monajjemi, M. Treating omicron BA.4 & BA.5 via herbal antioxidant asafoetida: A DFT study of carbon nanocarrier in drug delivery, J. Chil. Chem. Soc. 2023; *68*: 5781-5786.
40. Frisch MJ, Trucks GW, Schlegel HB, Scuseria GE, Robb MA, Cheeseman JR, et al. Gaussian 16, Revision C.01. Wallingford, CT: Gaussian, Inc.; 2016.
41. Vahabi V, Soleymanabadi H. A quantum mechanical analysis of the electronic response of BN nanocluster to formaldehyde. J Mex Chem Soc. 2016; 60: 34-39.
42. Rastgou A, Soleymanabadi H, Bodaghi A. DNA sequencing by borophene nanosheet via an electronic response: A theoretical study. Microelectron Eng. 2017; 169: 9-15.
43. Ochsenfeld C, Kussmann J, Koziol F. Ab initio NMR spectra for molecular systems with a thousand and more atoms: A linear-scaling method. Angew Chem. 2004; 116: 4585-4589.
44. Emwas AH, Szczepski K, Poulson BG, Chandra K, McKay RT, Dhahri M, et al. NMR as a “gold standard” method in drug design and discovery. Molecules. 2020; 25: 4597.
45. Smith JA. Nuclear quadrupole resonance spectroscopy. J Chem Educ. 1971; 48: 39-41.